Identification of Characteristic ELM Evolution Patterns with Alfvén-scale Measurements and Unsupervised Machine Learning Analysis

D. R. Smith[1], R. J. Fonck[1], G. R. McKee[1], A. Diallo[2], S. M. Kaye[2], D. M. Kriete[1], B. P. LeBlanc[2] and S. A. Sabbagh[3]

[1]University of Wisconsin-Madison, Madison, WI 53706, USA
[2]Princeton Plasma Physics Lab, Princeton, NJ 08543, USA
[3]Columbia University, New York, NY, 10027 USA

Corresponding Author: drsmith8@wisc.edu

Abstract:
The linear peeling-ballooning stability boundary expresses an onset condition for edge localized modes (ELMs), but ELM saturation mechanisms, filament dynamics, and multi-mode interactions require nonlinear models. In this contribution, characteristic ELM evolution patterns are identified and measured at Alfvén timescales with a beam emission spectroscopy (BES) diagnostic on NSTX, and parameter regimes corresponding to the characteristic ELM evolution patterns are identified. Clustering algorithms from the machine learning domain were applied to ELM time-series data, and the algorithms identified multiple groups of ELM events with similar evolution patterns. In addition, the identified ELM groups correspond to distinct parameter regimes for plasma current, shape, magnetic balance, and density pedestal profile. The observed evolution patterns and corresponding parameter regimes motivate nonlinear MHD simulations and suggest genuine variation in the underlying physical mechanisms that influence the evolution of ELM events. Finally, we present initial ELM observations from the 2D BES system on NSTX-U.

1 Introduction

The peeling-ballooning linear stability boundary expresses an onset condition for edge localized modes (ELMs) [1], but ELM saturation mechanisms, filament dynamics, and multi-mode interactions require nonlinear models [2, 3]. Understanding the nonlinear dynamics of ELM-induced heat and particle transport is a critical issue for ITER. Typical diagnostic tools for ELM observations, like Thomson scattering profiles and D_α filterscopes, do not resolve the Alfvén timescales of ELM events. Furthermore, heuristic ELM classification schemes (Type I, III, etc.) based on extrinsic ELM properties, like secular edge emission and inter-ELM period, do not capture the nonlinear dynamics and

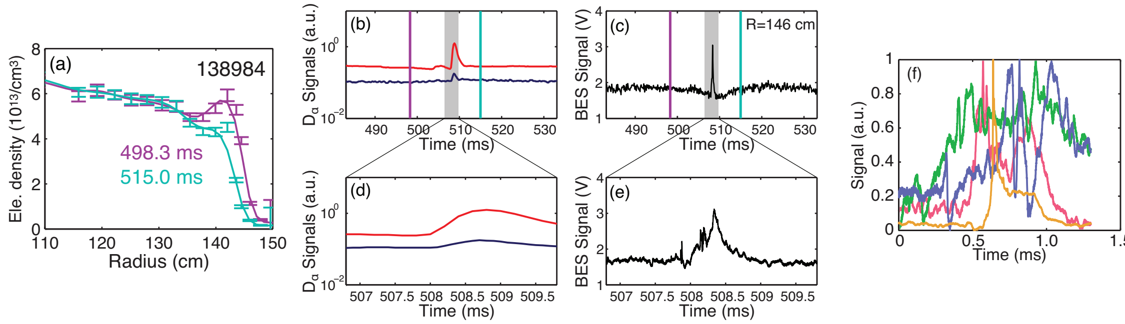

FIG. 1: (Color online) An example ELM event: (a) Thomson scattering profiles of electron density before and after the ELM event; (b) and (d) D_α filterscope signals viewing inner diverter (red) and full diverter (blue); and (c) and (e) BES measurements of the ELM event at $R = 146$ cm. In (b) and (c), vertical lines denote Thomson scattering measurement times. (f) Examples of diverse evolution dynamics for ELM events.

Alfvén-scale evolution of ELM events. Validation of nonlinear ELM models requires fast measurements on Alfvén timescales, and identification of common evolution patterns in ELM events can motivate the formulation or validation of nonlinear ELM models.

Recently, we investigated Alfvén-scale evolution patterns in ELM events captured by beam emission spectroscopy (BES) measurements on NSTX [4]. Unsupervised machine learning algorithms identified multiple groups of ELMs with distinct evolution characteristics. The identified ELM groups exhibited similar stored energy loss, but the groups occupy distinct regimes for several ELM-relevant parameters. The observed evolution patterns and associated parameter regimes suggest genuine variation in the underlying physical mechanisms that influence the evolution of ELM events and motivate nonlinear MHD simulations. In this contribution, we review the previous results for ELM evolution patterns and parameter regimes [4], and we present initial 2D BES measurements of an ELM event from NSTX-U.

2 Cluster Analysis of ELM Time Series Data

We identified 51 ELM events from the NSTX data archive with BES measurements that capture the Alfvén-scale nonlinear evolution of ELM events [4]. BES measurements of plasma density are localized with $\Delta x \approx 2$ cm and sample on Alfvén timescales at 2 MHz ($\Delta t = 0.5\,\mu$s, $\tau_A \sim 5\,\mu$s, and $\Delta t/\tau_A \sim 0.1$) [5, 6]. Figure 1(a-e) shows an example of ELM evolution dynamics captured by BES, Thomson scattering, and filterscope measurements. The ELM database was populated with the following objectives: 1) sample ELMs for a variety of machine and wall conditions, 2) identify ELMs that are isolated from other ELMs (ELM periods $\gtrsim 30$ ms) and confounding MHD activity, such as Alfvén avalanches, and 3) include only ELMs that exhibit a clear pedestal collapse or stored energy loss. The ELM events show stored energy losses up to 16%. An ELM pedestal collapse may not be observable if the ELM occurred early in the period between Thomson scattering

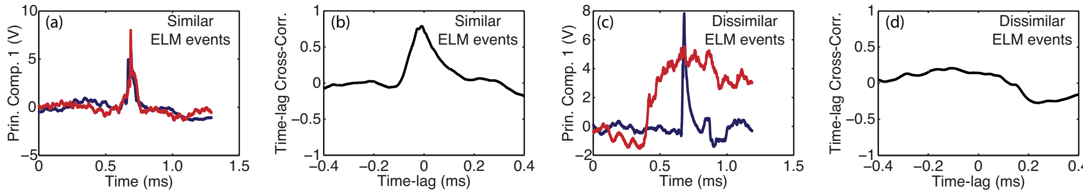

FIG. 2: (a,b) Similar ELMs exhibit a large maximum time-lag cross-correlation, and (c,d) dissimilar ELMs exhibit a small maximum time-lag cross-correlation.

measurements, and the stored energy loss may be erroneously small if the ELM occurred early in the period between magnetic reconstructions. Therefore, we require either a clear pedestal collapse or stored energy loss for ELMs in the database. The constraints likely exclude small, grassy, or Type V ELMs and Type III ELMs with periods $\lesssim$ 20 ms. In other words, the ELM database is likely populated only by Type I ELMs.

The ELM database spans a large range of plasma current, auxiliary heating power, plasma shape, and magnetic topology (for details, see Ref. [4]). To capture diverse ELM phenomena in a variety of machine conditions, the 51 ELM events were drawn from 34 H-mode discharges spanning four months of experimental operations. Measurements on Alfvén time-scales inherently capture the nonlinear dynamics and saturation mechanisms of ELM events, and Figure 1(f) shows examples of diverse evolution dynamics for ELM events in the database. For instance, some ELM events last less than 100 μs, but others persist up to 1 ms. A single perturbation dominates some ELM events, but other events show multiple perturbations. Finally, some events are oscillatory, but others are non-oscillatory. Identification of distinct groups of ELM evolution patterns may point to important nonlinear processes, so our first objective is to identify any structure or pattern in the ELM evolution database. Visual inspection may be adequate to identify structure in data, but visual inspection is not scalable to large or high-dimensional datasets. Unsupervised machine learning algorithms can identify structure, patterns, or organization in unlabeled data with computational speed and scalability.

We begin with unsupervised hierarchical clustering for the ELM dataset, and later we explore k-means clustering [7]. Hierarchical clustering links data objects in a multi-level hierarchy according to the degree of similarity [8]. The hierarchical clustering algorithm operates on a distance-like metric that quantifies dissimilarity between data objects, and the time series ELM data requires metrics that quantify dissimilarity between time series [9]. Time-series similarity metrics such as maximum time-lag cross-correlation, dynamic time warping, and maximum time-lag cross-correlation of wavelet-transformed signals were applied in this study. For example, Figure 2 shows ELMs with similar and dissimilar time-series evolution as determined by a cross-correlation dissimilarity metric. The hierarchical clustering algorithm operates on dissimilarity metrics, so maximum correlation values are converted to dissimilarity values with

$$D_{TLCC} \equiv 1 - \max(\rho(\tau)) \tag{1}$$

where $\rho(\tau)$ is the time-lag cross-correlation function and D_{TLCC} is the associated dissim-

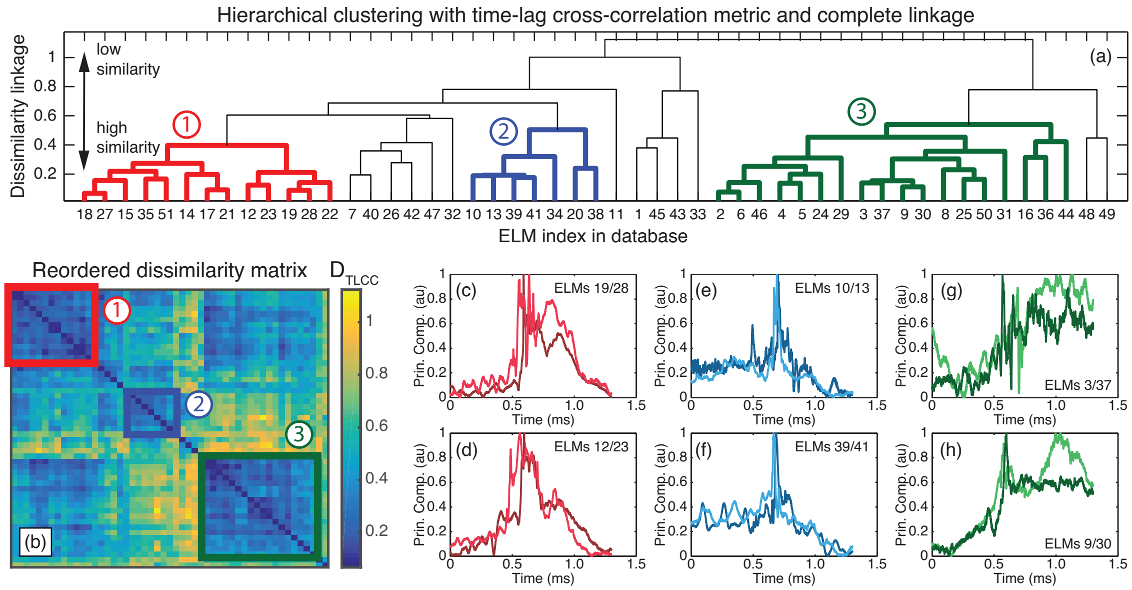

FIG. 3: (Color online) (a) Dendrogram showing hierarchical clustering in the ELM database with the time-lag cross-correlation dissimilarity metric and complete linkage, and (b) the dissimilarity matrix reordered for the ELM sequence in the dendrogram. Clusters 1 (red), 2 (blue), and 3 (green) denote groups of ELMs with similar evolution characteristics. (c-h) Examples of similar ELMs from the clusters.

ilarity metric.

The hierarchical clustering algorithm iteratively merges the most similar (least dissimilar) data objects into clusters, and the output is a multi-level hierarchy with the most similar objects linked at low levels. Dendrograms illustrate the multi-level hierarchy of data objects and clusters, and Figure 3(a) shows the dendrogram for the ELM database with complete linkage. Groups of data objects linked with low linkage values in the dendrogram are candidate clusters, and Figure 3(a) shows three candidate clusters labelled 1 (red), 2 (blue), and 3 (green). The designation of clusters in dendrograms is somewhat subjective, but good candidate clusters should preferably contain many members with high similarity inside the cluster and low similarity outside the cluster. In the reordered dissimilarity matrix, candidate clusters are square regions along the diagonal with low dissimilarity values, and the three candidate clusters are designated with colored squares in Figure 3(b). Figures 3(c-h) shows examples of ELM evolution for the identified clusters. ELMs in cluster 2 are short duration ($\sim$30 μs), and cluster 1 ELMs are similarly intense but with longer duration ($\sim$400 μs). Finally, ELMs in cluster 3 show elevated signals that persist over 1 ms. In summary, the clustering algorithm created a hierarchy of ELM events grouped by the degree of similarity. The modest results in Figure 3 are notable because 1) identifying structure, patterns, or association in data is a fundamental activity in scientific discovery; 2) algorithmic pattern recognition is scalable and readily automated; and 3) experimental fusion facilities generate large volumes of data. Hierar-

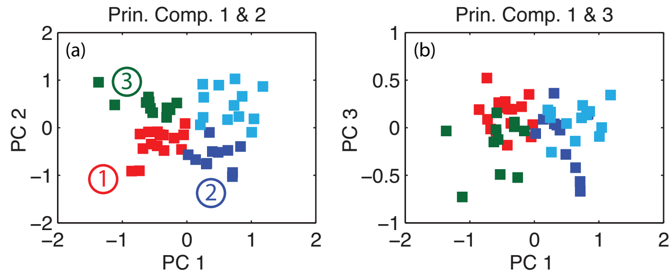

FIG. 4: K-means cluster results with four clusters for six benchmark ELMs. The clusters are plotted in principal component (PC) space to aid visualization: (a) clusters plotted in terms of PC 1 and PC 2, and (b) clusters plotted in terms of PC 1 and PC 3. The colors denote cluster membership.

chical clustering calculations with different similarity metrics and linkage formulas yield similar results, as described in Ref. [4].

Like hierarchical clustering, k-means clustering is an unsupervised learning algorithm that identifies structure, patterns, or association in data, but k-means clustering is divisive such that the dataset is divided into the specified number of clusters. For ELM time-series data, we designate a set of benchmark ELMs, and dissimilarity metrics for the benchmark ELMs serve as absolute coordinates in the k-means algorithm. The number of clusters is a specified parameter in the k-means algorithm, and the optimum cluster number is found through trial-and-error. Figure 4 illustrates the optimum four clusters, and the clusters are plotted in terms of principal components to facilitate visualization of high-dimensional data. Clusters 1, 2, and 3 in Figure 4 correspond to the same clusters in Figure 3, but the cyan cluster in Figure 4 has no corresponding low-linkage cluster in Figure 3. For this reason, we are reluctant to attached "cluster 4" designation to the cyan cluster in Figure 4.

The k-means clustering results in Figure 4 indicate four clusters are optimal, but the hierarchical clustering results in Figure 3 point to three clusters of ELMs with similar evolution. The apparent discrepancy is resolved by mapping k-means results to the hierarchical results. As discussed in Ref. [4], the clusters from k-means clustering in Figure 4 largely map to clusters previously identified from hierarchical clustering in Figure 3. The cyan cluster from k-means analysis in Figure 4 maps to a group of ELMs that are largely unlike all other ELMs from hierarchical analysis in Figure 3. In other words, k-means clustering captures the three clusters identified in hierarchical results plus a fourth cluster of ELMs (cyan) that defied grouping in the hierarchical results.

3 Parameter regimes for ELM clusters

Unsupervised clustering techniques identified three clusters of ELMs with similar evolution patterns in the previous section, and now we search for ELM-relevant parameters that correlate with the identified ELM clusters. Stored energy loss is a key metric for

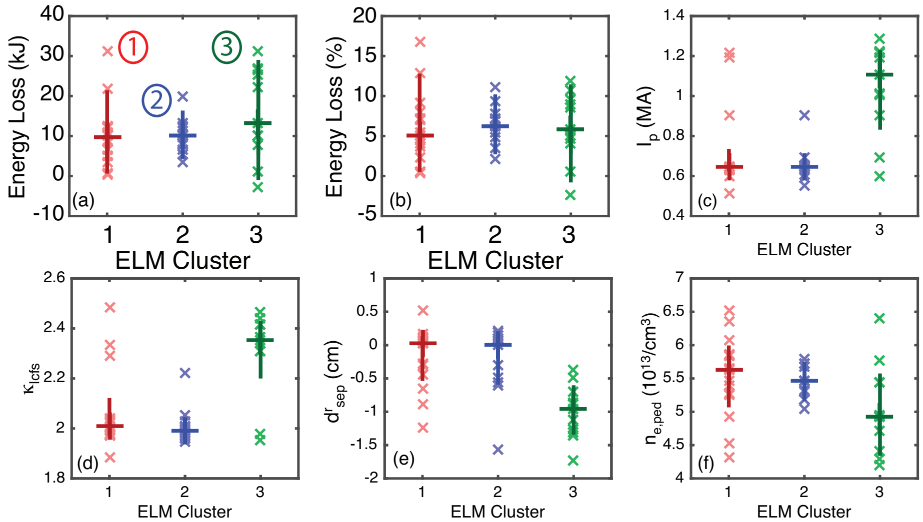

FIG. 5: Stored energy losses for the ELM clusters in (a) kJ and (b) % loss; (c) plasma current; (d) elongation; (e) magnetic balance ($d^r_{sep} < 0$ is lower single null); and (f) pedestal density height. The small x's are individual ELMs, the solid bars are mean, 20th, and 80th percentile values. The 20th–80th percentile range captures typical parameter values.

ELMs [10], but Figure 5(a,b) indicates the identified ELM clusters exhibit similar stored energy losses. The ELM clusters do not appear to correlate with stored energy loss, but Figure 5(c-f) shows that the ELM clusters do correlate with several ELM-relevant parameters such as plasma current, elongation, magnetic balance, and pedestal density height. Based on the observed evolution patterns and parameter regimes, we expect the identified parameters will influence the evolution patterns and nonlinear dynamics in ELM simulations. A more comprehensive discussion of ELM clusters and parameter regimes can be found in Ref. [4].

If Figure 5(c), cluster 3 with prolonged elevated signals corresponds to higher I_p, and clusters 1 and 2, with shorter durations, correspond to lower I_p. The clustering with I_p is reminiscent of the fast and slow post-ELM pedestal temperature gradient recoveries observed in DIII-D [11]. In terms of geometry and magnetic balance, cluster 3 occurs preferentially at higher elongation (κ) and in lower single null configurations ($dR_{sep} \lesssim -0.5$ cm), and clusters 1 and 2 occur preferentially at lower elongation and double null configurations. The variations in ELM evolution could be due to geometry or magnetic topology variations, but regardless an accurate nonlinear model of ELM dynamics should capture variations in ELM evolution due to any factor including geometry or topology. Note, however, that the ELM database lacks observations in the upper single null configuration. In strongly shaped plasmas, higher density shifts the dominant peeling-ballooning mode to higher-n ballooning modes [12]. In Figure 5, the dominance of clusters 1 and 2 at higher pedestal density values could be associated with a shift to higher-n ballooning modes.

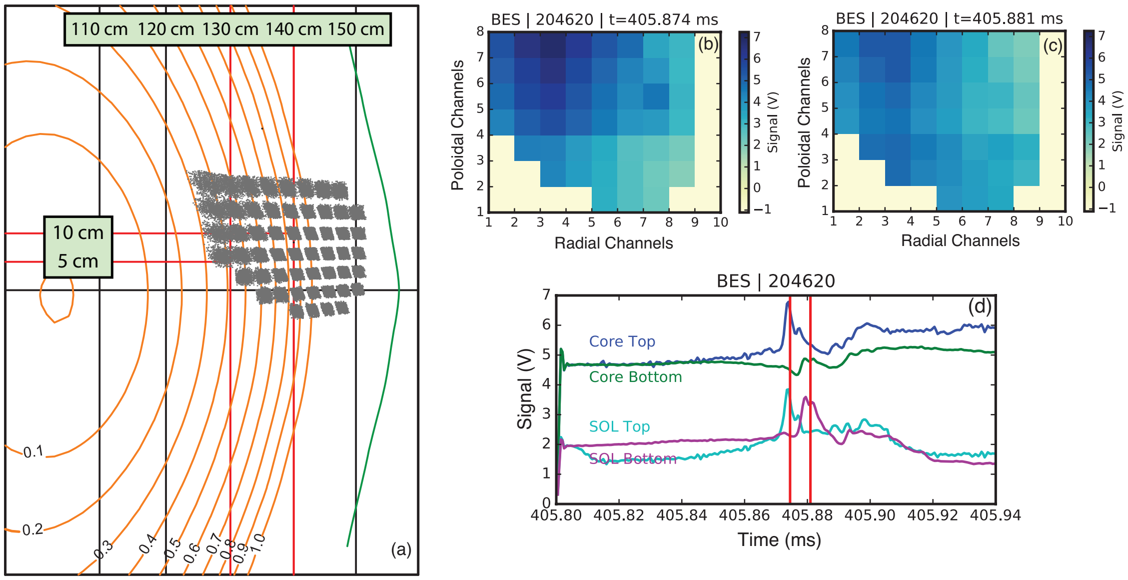

FIG. 6: (a) Layout of the reconfigured 2D BES system on NSTX-U, (b, c) 2D BES measurements from NSTX-U of an ELM structure propagating downward, and (d) time-series evolution from multiple regions in the 2D BES region of coverage.

4 2D ELM imaging on NSTX-U

The BES system on NSTX was expanded and upgraded for NSTX-U. Specifically, the detection system [5, 6] was expanded from 32 to 48 detection channels, and a further expansion to 64 detection channels is planned. Also, the sightline layout was reconfigured for 2D imaging in the pedestal region. Figure 6(a) shows the reconfigured 2D coverage with 54 sightlines spanning the outer plasma and scrape-off-layer regions. BES measurements from the inaugural operations of NSTX-U captured the 2D, Alfvén-scale evolution of an ELM event. Figures 6(b,c) shows an ELM structure moving down the field of view, and Figure 6(d) shows the time-series evolution of the ELM event at four regions. 2D BES measurements on NSTX-U provides new opportunities to investigate the nonlinear dynamics of turbulence, ELMs, Alfvén eigenmodes, and other fast instabilities.

5 Summary

We implemented unsupervised machine learning algorithms that identified characteristic evolution patterns in a database of ELM events. Time-series similarity metrics quantified the similarity among ELM time-series data, and clustering algorithms identified two and possibly three clusters of ELMs with similar evolution characteristics. The identified ELM clusters triggered similar stored energy loss (Figure 5), but the clusters occupied distinct parameter regimes for ELM-relevant parameters like plasma current, magnetic balance, triangularity, and pedestal height. The distinct evolution patterns and parameter regimes point to genuine variations in the underlying nonlinear dynamics. Based on the observed evolution patterns and parameter regimes, we expect the identified parameters will influence the evolution patterns and nonlinear dynamics in ELM simulations. Finally, 2D BES measurements on NSTX-U provides new opportunities to investigate the nonlinear dynamics of ELMs and other fast instabilities.

6 Acknowledgements

This material is based upon work supported by the U.S. Department of Energy, Office of Science, Office of Fusion Energy Sciences under Award Numbers DE-FG02-89ER53296, DE-SC0001288, and DE-AC02-09CH11466. This research used resources of the National Spherical Torus Experiment-Upgrade, which is a DOE Office of Science User Facility.

References

[1] P. B. Snyder, H. R. Wilson, T. H. Osborne, and A. W. Leonard, Plasma Phys. Control. Fusion **46**, A131 (2004).

[2] X. Q. Xu, B. D. Dudson, P. B. Snyder, M. V. Umansky, H. R. Wilson, and T. Casper, Nucl. Fusion **51**, 103040 (2011).

[3] M. Holzl, S. Gunter, R. P. Wenninger, *et al.*, Phys. Plasmas **19**, 082505 (2012).

[4] D. R. Smith, R. J. Fonck, G. R. McKee, A. Diallo, S. M. Kaye, B. P. LeBlanc, and S. A. Sabbagh, Plasma Phys. Control. Fusion **58**, 045003 (2016).

[5] D. R. Smith, H. Feder, R. Feder, R. J. Fonck, G. Labik, G. R. McKee, N. Schoenbeck, B. C. Stratton, I. Uzun-Kaymak, and G. Winz, Rev. Sci. Instrum. **81**, 10D717 (2010).

[6] D. R. Smith, R. J. Fonck, G. R. McKee, and D. S. Thompson, Rev. Sci. Instrum. **83**, 10D502 (2012).

[7] R. Xu and D. Wunsch, IEEE Transactions on Neural Networks **16**, 645 (2005).

[8] M. B. Eisen, P. T. Spellman, P. O. Brown, and D. Botstein, Proc. Natl. Acad. Sci. USA **95**, 14863 (1998).

[9] T. W. Liao, Pattern Recognition **38**, 1857 (2005).

[10] S. Sabbagh, S. Kaye, J. Menard, F. Paoletti, M. Bell, *et al.*, Nucl. Fusion **41**, 1601 (2001).

[11] A. Diallo, R. J. Groebner, T. L. Rhodes, D. J. Battaglia, D. R. Smith, T. H. Osborne, J. M. Canik, W. Guttenfelder, and P. B. Snyder, Phys. Plasmas **22**, 056111 (2015).

[12] P. B. Snyder, K. H. Burrell, H. R. Wilson, M. S. Chu, M. E. Fenstermacher, *et al.*, Nucl. Fusion **47**, 961 (2007).